# Recycled cement thermoactivated at different temperatures

Sofia Real[1,*], Ana Carriço [2], José Alexandre Bogas [3], Mafalda Guedes [4]

1. PhD, CERIS, Instituto Superior Técnico, Universidade de Lisboa
2. MSc, CERIS, Instituto Superior Técnico, Universidade de Lisboa
3. PhD, CERIS, Instituto Superior Técnico, Universidade de Lisboa
4. PhD, CDP2T and Department of Mechanical Engineering, Setúbal School of Technology, Instituto Politécnico de Setúbal, 2910-761 Setúbal, Portugal; CeFEMA, Instituto Superior Técnico, Universidade de Lisboa

[*]Corresponding author email: sofia.real@tecnico.ulisboa.pt

## Abstract

This paper discusses the effect of the thermal activation temperature on the rehydration of recycled cement and mechanical strength of pastes produced with this more eco-efficient binder. For this purpose, various tests were performed in order to characterise the thermoactivated recycled cement, namely thermogravimetry, X-ray diffraction, and $^{29}Si$ nuclear magnetic resonance spectroscopy, as well as water demand, setting time and isothermal calorimetry. The mechanical strength of the recycled cement pastes was also determined. Overall, the dehydration and hydration of the thermoactivated recycled cement were significantly affected by the thermoactivation temperature, leading to the formation of distinct $C_2S$ polymorphs. The compressive strength of the thermoactivated recycled cement pastes was influenced by the different reactivity of these polymorphs. These binders presented longer setting times and their pastes displayed lower compressive strength than those with the reference CEM I. This was essentially attributed to the high water demand and pre-hydration phenomena exhibited by the thermoactivated recycled cement. The optimal thermal activation temperature was 700 ºC.

***Keywords:*** *Recycled cement, Thermal activation, Rehydration.*

## 1. Introduction

In last decades, the construction industry has tried to follow the path of sustainable development by exploring innovative eco-efficient solutions, that could reduce the major environmental problems associated to concrete production. To achieve this goal, investigation works have focused on concrete recycling, mainly applied in the form of recycled aggregates or fillers, partially replacing natural aggregates and cement, respectively. More recently, the potential of the thermal activation in recovering the rehydration ability of recycled cement has been explored.

The high water demand and low setting time appear to be the main concerns of thermoactivated recycled cement binders (RB). Nonetheless, so far, the reason for this behaviour and the effect of the treatment temperature have not been entirely explained. Various authors have described that the water demand increased linearly with the thermal activation temperature (Shui et al., 2009; Vyšvaril et al., 2014). This tendency has been attributed to the elevated surface area of RB (Baldusco et al., 2019), to their free CaO content (Shui et al., 2009), to their particle absorption (Zhang et al., 2018) and to particle agglomeration (Yu and Shui, 2013). The short setting times of these binders have been ascribed to their quick rehydration, as a result of their surface area and reactivity (Baldusco et al., 2019; Shui et al., 2009; Zhang et al., 2018). Additionally, several authors have pointed out the reduction of the setting time with the thermal activation temperature, until 800 ºC. However, different explanations have been suggested, such as the growing dehydration (Shui et al., 2009) and free CaO content of RB (Serpell and Lopez, 2015; Vyšvaril et al., 2014) or even a false setting phenomenon resulting from the rapid hydration of free CaO

(Serpell and Lopez, 2015). On the other hand, Bogas et al. (2019) and Carriço et al. (2020) reported cases where RB displayed longer setting times than the reference CEM I. The results were justified with RB particle agglomeration and a precocious hydration phenomenon of this type of binder, throughout the cooling and storing phases.

The composition of the recycled cement phases with thermal activation is yet to be completely explained. Alonso and Fernandez (2004) resorted to nuclear magnetic resonance spectroscopy ($^{29}$Si-NMR) to demonstrate the creation of a different nesosilicate over 200ºC, that was not as crystalline as the $C_2S$ polymorph present in the reference cement. Lü et al. (2008) combined $^{29}$Si-NMR and X-ray diffraction analysis (XRD) to study the phases composition of RB, having concluded that the polymorph β-$C_2S$ was formed over 650 ºC, turning into an exceedingly crystalline phase of reduced reactivity at 900ºC. Carriço et al. (2020) described the formation of $C_2S$ polymorph similar to α'$_L$-$C_2S$ in RB treated over 600 ºC, using XRD analysis. Serpell and Zunino (2017) reported the coexistence of two $C_2S$ polymorphs, α'$_H$-$C_2S$ of high reactivity and also β-$C_2S$, over 740 ºC, having mentioned the predominance of the first until 800 ºC and of the latter at 900 ºC. Shui et al. (2014) recognised two $C_2S$ polymorphs over 800 ºC, α-$C_2S$ and β-$C_2S$.

Altogether, thermoactivated recycled cement binders have become a viable eco-efficient option. However, the knowledge in this research area is still limited.

This paper aims to characterise the rehydration behaviour and compressive strength of recycled cement binders subjected to varying treatment temperatures. In order to achieve this purpose, a vast experimental campaign was carried out, comprising the production and testing of recycled cement binders thermoactivated between 400 and 900 ºC, through thermogravimetric (TG) analysis, XRD analysis, $^{29}$Si-NMR analysis, water demand, setting time, isothermal calorimetry and compressive strength.

# 2. Experimental programme

## 2.1. Production of thermoactivated recycled cements and respective pastes

The source paste was produced with CEM I 42.5R and a water/cement ratio (w/c) of 0.55, having reached a 28-days compressive strength of about 41 MPa. The source paste was cured in a 95% RH environment for up to a week and then stored in laboratory environment for more than three months. Afterwards, the source paste underwent a series of crushing, grinding and milling processes in order to reduce its particle size, and then was sieved to obtain non-treated particles under 250 μm (NT). Subsequently, resorting to a Thermolab Scientific Equipments' rotary tube furnace, these particles were subjected to thermal activation, by heating at 10 ºC/min up to the treatment temperature, remaining at this level for 3 hours and then cooling inside the oven. In order to comprise the different dehydration stages of cement paste, the following treatment temperatures were selected: 400, 500, 600, 700, 800 and 900 ºC. The obtained thermoactivated recycled cements were designated B400-B900, according to their treatment temperature. These binders were used to produce pastes with a water/binder ratio (w/b) that enabled normal consistency (EN 196-3, 2016), which were designated PB400-PB900, according to the thermal activation temperature of the binder (Table 1). Moreover, other pastes were also produced with NT (PNT) and CEM I (PC0.72 and PC0.31), for comparison (Table 1). The production of these pastes consisted on mixing each binder with water for about 8 mins.

Table 1. Composition of the produced pastes

| **Paste designation** | PC0.31 | PC0.72 | PNT | PB400 | PB500 | PB600 | PB700 | PB800 | PB900 |
|---|---|---|---|---|---|---|---|---|---|
| **Binder designation** | CEM I | CEM I | NT | B400 | B500 | B600 | B700 | B800 | B900 |
| **w/b** | 0.31 | 0.72 | 0.43 | 0.62 | 0.68 | 0.73 | 0.72 | 0.87 | 0.91 |

### 2.2. Test methods

The thermoactivated recycled cement binders were characterised with respect to their rehydration behaviour and compressive strength. The XRD analysis was performed on a *PANalytical X'Pert Pro* diffractometer with CuKα radiation, for a 2θ scanning range of 5-60º, a step size and time of 0.03º and 100 s, respectively. The $^{29}$Si-NMR analysis was performed on a *TecMag/Bruker 300* "wide bore" spectrometer with a 5 kHz spinning and a 20 s relaxation delay, for 250 scans, at a 59.595 MHz $^{29}$Si resonance. Moreover, tetrakis (trimethyl sylil) silane ($^{29}$Si = -9.8; -135.64 ppm) was used as external reference. The thermogravimetric (TG) analysis was accomplished in a *PC LUXX Thermobalance*, at a constant heating rate of 25 ºC/min until 1000 ºC, under a nitrogen gas flow of 150 mL/min. The combined water ($W_b$) and the hydration degree ($\alpha_{TG}$) of the binders and pastes were estimated as suggested in Bogas et al. (2019). The calcium hydroxide (CH) and CaO contents of the RB were estimated through Eqs. (1) and (2), where Ldx and Ldc are the weight losses (WL) corresponding to the dehydroxylation of CH and the decarbonation of carbonated phases and $Ldx_{NT}$ and $Ldc_{NT}$ are correcting factors that account for these WL in the source paste and $M_{CH}$, $M_{H2O}$, $M_{CO2}$ and $M_{CaO}$ correspond to the molecular weights of CH, $H_2O$, $CO_2$ and CaO, respectively.

$$CH = L_{dx} \times \frac{M_{CH}}{M_{H_2O}} + \left(L_{dc} - L_{dc_{NT}}\right) \times \frac{M_{CH}}{M_{CO_2}} \quad (1)$$

$$CaO = \left(L_{dx_{NT}} - L_{dx}\right) \times \frac{M_{CaO}}{M_{H_2O}} + \left(L_{dc_{NT}} - L_{dc}\right) \times \frac{M_{CaO}}{M_{CO_2}} \quad (2)$$

The water demand and setting time of the binders were assessed according to EN 196-3 (2016). The isothermal calorimetry was performed on a *TAM Air-8 channels* equipment, according to EN 196-11: Method A (external mixing) (EN 196-11, 2018). The samples were produced with a w/b of about 1.0 and placed in the calorimeter within 4 mins after mixing. The recording of the released heat only began after about 45 mins, with the thermal stabilisation of the apparatus and continued up to 7 days. The compressive strength test of the pastes was performed on three 16×4×4 cm$^3$ prisms per composition and age, up to 90 days, according to EN 1015-11 (2000). The prisms were produced and stored in a 95%RH chamber, until testing age.

## 3. Results and discussion

### 3.1. Thermogravimetric analysis

Figure 1 displays the TG and first derivative curves of CEM I, NT and B400-B900. The WL of CEM I are typical of gypsum decomposition, at about 140 ºC, and decarbonation of lime filler, at around 700-800 ºC, whereas the WL of NT pertain to the dehydration of calcium silicate hydrates (C-S-H) and decomposition of aluminate phases (< 470 ºC), dehydroxylation of calcium hydroxide (CH) (470-565ºC) and decarbonation of carbonated compounds (> 565 ºC) (Alonso and Fernandez, 2004; Bogas et al., 2019; Wang et al., 2018). The $\alpha_{TG}$ of NT was about 76 % (Table 2), representing a well-hydrated cement paste.

Up to 400 ºC, the RB did not present significant WL, due to the fact that these binders underwent similar to higher temperatures during thermal treatment. Between 400 and 600 ºC, the RB experienced considerable WL, either owed to remaining CH from NT after thermal treatment, in B400 and B500, or to precocious hydration of CaO to form CH, during the cooling/storing phases, in B600-B900. Additionally, the dehydroxylation of CH occurred over a larger temperature range in NT and B400-B500 than in B600-B900 (Fig. 2), indicating that RB subjected to higher treatment temperatures contained CH of lower bonding energy, stemming from the rehydration of CaO. Over 600 ºC, except for B800-B900, which underwent significant decarbonation during thermal treatment, the RB tended to display increasing WL compared to NT, implying that carbonation might have occurred upon thermal treatment. In general, the reduction of CH content was complemented by the increase of CaO content, mainly due to the dehydroxylation of CH (up to 600ºC) and to the decarbonation of carbonated compounds (over 600ºC) (Table 2). Furthermore, the effectiveness of the thermal treatment was demonstrated by the reduction of the $W_b$ with the treatment temperature compared to NT. Noteworthy is the fact that, in B600-B900, the $W_b$ was as high as 4% that could hinder their rehydration capacity.

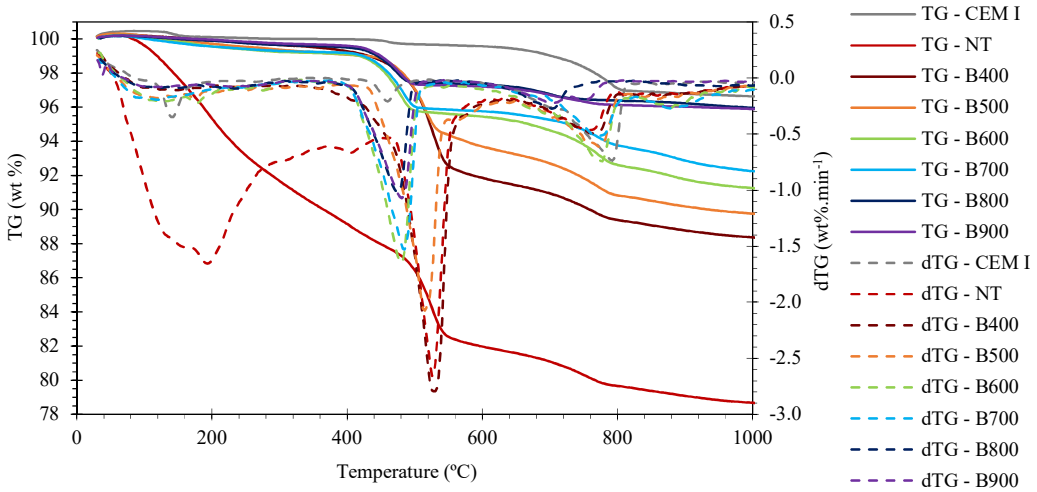


Figure 1. TG and first derivative (dTG) curves of CEM I, NT and B400-B900

Table 2. Calculated $W_b$, $\alpha_{TG}$, CH and CaO contents of CEM I, NT and B400-B900

| **Binder designation** | CEM I | NT | B400 | B500 | B600 | B700 | B800 | B900 |
|---|---|---|---|---|---|---|---|---|
| **$W_b$ (%)** | 0.30 | 17.37 | 7.20 | 4.90 | 4.10 | 4.00 | 2.50 | 2.60 |
| **$\alpha_{TG}$ (%)** | 1.30 | 75.53 | 31.30 | 21.30 | 17.83 | 17.39 | 10.87 | 11.30 |
| **CH (wt%)** | 0.82 | 18.16 | 18.10 | 15.22 | 13.16 | 13.16 | 8.23 | 9.05 |
| **CaO (wt%)** | - | - | - | - | 3.67 | 4.84 | 11.46 | 10.90 |

## 3.2. X-ray diffraction analysis

Figure 2 displays the XRD analyses of CEM I, NT and B400-B900. As expected, the main crystalline phases of clinker were identified in CEM I, namely β-$C_2S$, $C_3S$ and gypsum (Fig. 2a). The typical crystalline phases of hydrated cement pastes were detected in NT, namely C-S-H, CH and ettringite, and also $CaCO_3$ and other carbonated aluminate compounds, which should have resulted from the carbonation of the NT during milling and/or storing (Fig. 2b).

The XRD of B400 and B500 (Figs. 2c-d) established the decomposition of some hydrated crystalline phases, namely the inexistence of ettringite and the transformation of C-S-H into tobermorite 9 Å. Over 600 ºC, the presence of $C_2S$ polymorphs was detected (Figs. 2e-h), resulting from the depolymerisation of C-S-H. The wide width of the $C_2S$ peaks between 30º and 35º implied that this compound was not completely crystallised. The low intensity peaks at 53.5º-56º identified in B600 and B700 (Figs. 2e-f), indicated that this polymorph was α'$_L$-$C_2S$. In B800 and B900 (Figs. 2g-h), besides the more defined and intense α'$_L$-$C_2S$ peaks, associated to its high crystallinity, β-$C_2S$ peaks were also detected, suggesting the formation of $C_2S$ polymorphs of lower reactivity over 800 ºC (Lü et al., 2008; Serpell and Lopez, 2015; Wang et al., 2018).

Unexpectedly, B600-B800 (Figs. 2e-g) displayed CH and, in B600-B700, the presence of CaO was not detected, even though, at this treatment temperature range, the complete dehydroxylation of CH should have taken place. This corroborates the TG results (Fig. 1, Table 2), indicating that the precocious hydration of these binders may have occurred. Overall, the XRD of RB also marked the presence of $CaCO_3$, stemming from the carbonation of source paste.

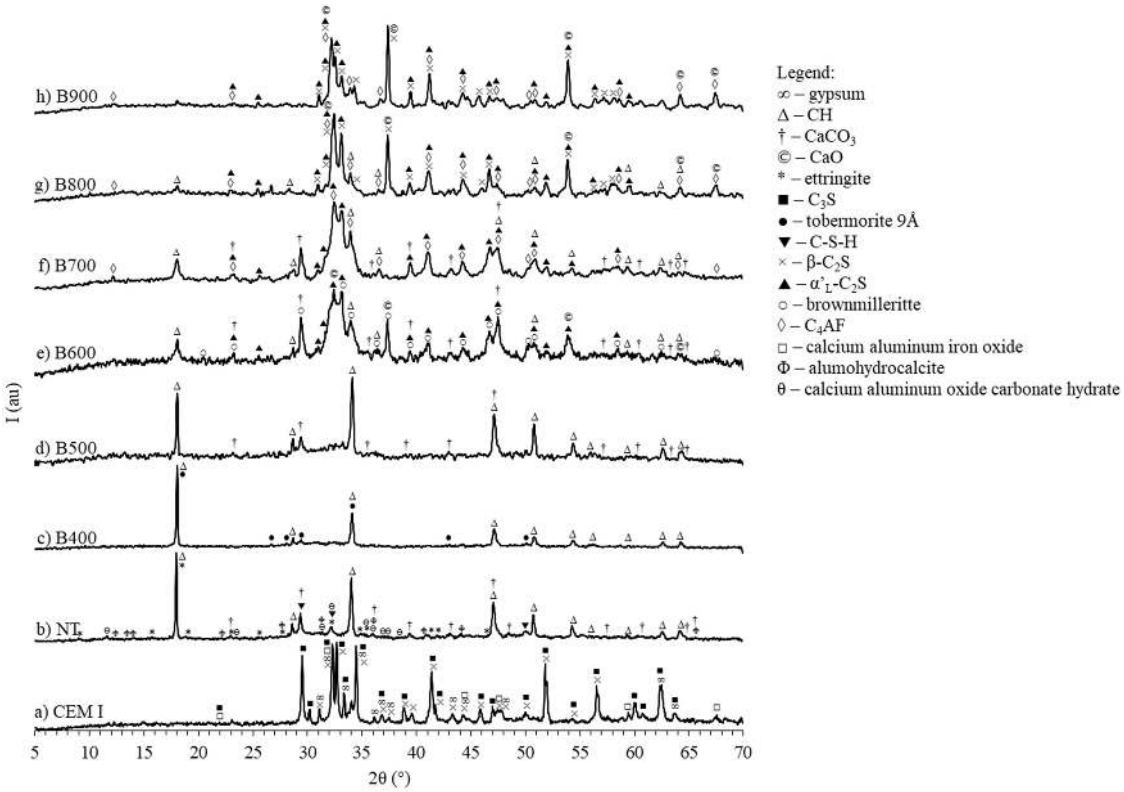


Figure 2. XRD analysis of CEM I, NT and B400-B900

### 3.3. Nuclear magnetic resonance spectroscopy

Figure 3 displays the $^{29}$Si-NMR spectra of CEM I, NT and B400-B900. The $^{29}$Si-NMR analysis of CEM I (Fig. 3a) revealed two main $Q^0$ peaks (Table 3), indicating the presence of monomeric orthosilicates, commonly found in CEM I (Alonso and Fernandez, 2004; Skibsted, 2016), which should correspond to the β-$C_2S$ and $C_3S$, obtained in the XRD analysis (Fig. 2a).

The $^{29}$Si-NMR analysis of NT showed four main $Q^n$ peaks (Fig. 3b, Table 3). The two $Q^0$ peaks of lower intensity than those of CEM I represent the residual anhydrous calcium silicates from CEM I, namely the polymorph β-$C_2S$ of typically slow reactivity (Alonso and Fernandez, 2004). The $Q^1$ peaks represent the end-chain group associated to the polymerisation of C-S-H, whereas the $Q^2$ peaks represent the middle-chain group.

The dehydration and depolymerisation of C-S-H with the treatment temperature was substantiated by the gradual reduction of $Q^1$ and $Q^2$ peak intensity and increase of $Q^0$ peak intensity (Fig. 3, Table 3). Though the $^{29}$Si-NMR analysis of B400 also revealed four main $Q^n$ peaks at chemical shifts similar to those of NT (Fig. 3c, Table 3), the reduction of the $Q^2/Q^1$ ratio indicates the presence of C-S-H with a shorter chain length, consistent with the decomposition of these hydration products.

Over 600 ºC, no $Q^1$ or $Q^2$ peaks were detected, corroborating the full depolymerisation of C-S-H and the formation of anhydrous calcium silicates, as previously mentioned in the XRD analyses (Fig. 2). The same was reported by Lü et al. (2008), in RB thermoactivated over 700 ºC. In the $^{29}$Si-NMR of B600 (Fig. 3d) and B700 (Fig. 3e), a main $Q^0$ peak was identified at -71.35 ppm, which is typically ascribed to the polymorph β-$C_2S$ (Grimmer et al., 1985; Skibsted, 2016). Nevertheless, the XRD analyses of B600-B700 only identified the polymorph α'$_L$-$C_2S$ (Figs. 2e-f). Moreover, according to Hong and Young (1999), the polymorph α'$_L$-$C_2S$ also exhibited a main $Q^0$ peak at -71 ppm. Consequently, it could be confused with the polymorph β-$C_2S$, due to the fact that the chemical shift of anhydrous calcium silicates is extremely influenced by the conditions in which they were formed and

stabilised (Grimmer et al., 1985). Thus, in this study, this $Q^0$ peak was associated with the polymorph $\alpha'_L$-$C_2S$.

The $^{29}$Si-NMR analysis B800 (Fig. 3f) detected a $Q^0$ peak at a different chemical shift (-70.60 ppm), that is in accordance with the formation of the polymorph β-$C_2S$ (Carriço et al., 2020; Grimmer et al., 1985; Serpell and Zunino, 2017), as shown in the XRD analysis (Fig. 2g). In B900 (Fig. 3g), this $Q^0$ peak became finer and more intense than in B800. In general, the $Q^0$ peaks became progressively sharper with the increment of thermal activation temperature, representing a more crystalline compound, which is in accordance with the XRD analysis (Fig. 2).

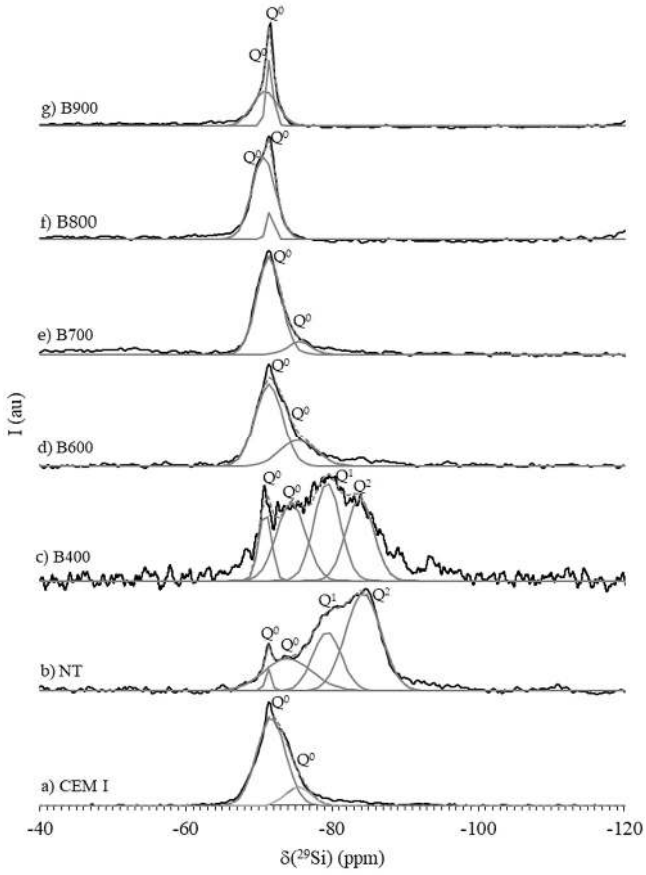


Figure 3. $^{29}$Si-NMR spectra of CEM I, NT and B400-B900

Table 3. Isotropic chemical shifts ($\delta^{29}$Si) for CEM I, NT and B400-B900

| Binder designation | Structural unit | δ($^{29}$Si) (ppm) |
|---|---|---|
| CEM I | $Q^0$ | -71.67 |
| | $Q^0$ | -75.40 |
| NT | $Q^0$ | -71.27 |
| | $Q^0$ | -73.98 |
| | $Q^1$ | -79.33 |
| | $Q^2$ | -84.31 |
| B400 | $Q^0$ | -70.86 |
| | $Q^0$ | -74.40 |
| | $Q^1$ | -79.33 |
| | $Q^2$ | -83.80 |
| B600 | $Q^0$ | -71.35 |
| | $Q^0$ | -75.42 |
| B700 | $Q^0$ | -71.35 |
| | $Q^0$ | -75.60 |
| B800 | $Q^0$ | -71.56 |
| | $Q^0$ | -70.60 |
| B900 | $Q^0$ | -71.46 |
| | $Q^0$ | -70.81 |

## 3.4. Water demand and setting time

Table 4 presents the water demand and setting time of CEM I and B400-B900. The water required to reach normal consistency in PB400-PB900 varied between 0.62 and 0.91, having been up to 3 times higher than that of the CEM I paste (0.31).

Table 4. Water demand and setting time of CEM I, NT and B400-B900

| **Paste designation** | | PC0.31 | PNT | PB400 | PB500 | PB600 | PB700 | PB800 | PB900 |
|---|---|---|---|---|---|---|---|---|---|
| **Binder** | | CEM I | NT | B400 | B500 | B600 | B700 | B800 | B900 |
| **Water demand (w/b)** | | 0.31 | 0.43 | 0.62 | 0.68 | 0.73 | 0.72 | 0.87 | 0.91 |
| **Setting Time (mins)** | **Initial** | 85 | - | 145 | 165 | 193 | 315 | 360 | >720 |
| | **Final** | 115 | - | 265 | 295 | 275 | 417 | 460 | >1440 |

Moreover, the water demand of the RB pastes increased with the treatment temperature (Table 4), which is in accordance with the literature (Shui et al., 2009; Vyšvaril et al., 2014; Wang et al., 2018). This could be explained by the increase of the particle surface area and the formation of free CaO (Table 2) in these binders (Shui et al., 2009). The free CaO reacts instantly upon contact with a portion of the mixing water, whereas another portion evaporates as a result of this exothermic reaction. Furthermore, the increment of RB particle porosity with the treatment temperature, increasing water absorption, should also have contributed to these results (Baldusco et al., 2019; Zhang et al., 2018).

B400-B800 exhibited initial and final setting times between 145 and 360 min and between 265 and 460 min, respectively. In contrast with the literature (Bogas et al., 2019; Shui et al., 2009; Vyšvaril et al., 2014), the setting times of RB pastes were over 2 times higher than that of CEM I, having increased with the treatment temperature (Table 4). The setting times of RB pastes are frequently described as significantly lower than those of CEM I, due to the fast rehydration of these binders of high surface area and reactivity (Baldusco et al., 2019; Shui et al., 2009; Zhang et al., 2018). Additionally, several authors have recounted the decrease of the setting time of RB pastes with the thermal activation temperature until 800 ºC (Baldusco et al., 2019; Shui et al., 2009; Zhang et al., 2018). This tendency was justified by the increasing free CaO content (Vyšvaril et al., 2014), which may also be accountable for an early false setting phenomenon (Serpell and Lopez, 2015).

In this study, the fact that part of the CaO content in the RB were pre-hydrated may have delayed the setting times of these binders. Noteworthy is the significant increase of the setting time over 800ºC, (Table 4), confirming the relevant reduction of the RB reactivity.

### 3.5. Isothermal calorimetry

Figure 4 shows the heat flow over time of pastes produced with CEM I, NT and B400-B900 and a w/b of 1.0. In the initial hydrolysis stage, the heat rate of the RB pastes generally decreased with the treatment temperature, having been up to 2.6 times higher than the heat rate of the paste with CEM I. Similar findings were presented by other authors (Angulo et al., 2013; Baldusco et al., 2019; Bogas et al., 2019; Zhang et al., 2018). If the first 45 mins had been recorded, this difference would have been significantly higher (Baldusco et al., 2019; Zhang et al., 2018). Several possible explanations for this phenomenon have been put forward, namely the high surface area of RB and their predisposition to rapidly re-polymerise (Shui et al., 2009), as well as its elevated calcium aluminate content (Baldusco et al., 2019) and the exothermic reaction of CaO with water (Angulo et al., 2013; Bogas et al., 2019; Wang et al., 2018).

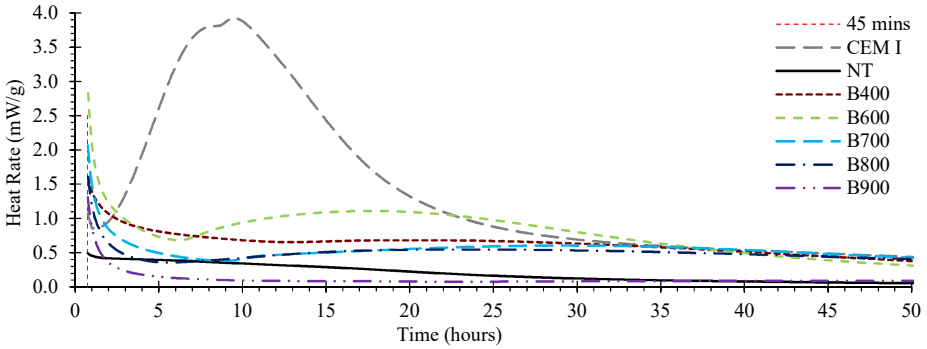


Figure 4. Heat flow over time of pastes with CEM I, NT and B400-B900 and a w/b of 1.0

Both RB and CEM I pastes displayed similar hydration stages, namely induction, acceleration and deceleration, though the time period and heat rate associated to each stage were significantly different (Fig. 4). The RB required considerably longer periods to reach the beginning and peak of acceleration stage than the reference CEM I paste. Moreover, throughout this stage, RB pastes displayed maximum heat rates over 3 times lower than that of the reference CEM I paste. The maximum heat rate increased with the treatment temperature up to 600ºC and then decreased up to 900ºC. This tendency is in accordance with the findings of other authors (Angulo et al., 2013; Baldusco et al., 2019; Bogas et al., 2019; Wang et al., 2018).

At this temperature range, the free CaO and calcium aluminates react rapidly with water and hydration of the new $C_2S$ polymorph occurs. However, the elevated initial hydration heat should not be solely ascribed to free CaO hydration, due to the fact that the free CaO content increased with the thermal activation temperature unlike the heat release (Table 2). This phenomenon should have also derived from the reactivity of the new compounds formed during thermal treatment.

The pastes with NT, B400 and B900 did not promote noteworthy hydration heat release. Indeed, given that NT was well-hydrated prior to mixing, the minor hydration heat released by its paste could be attributed to the hydration of residual anhydrous compounds, as also found by Angulo et al. (2013). The flat acceleration stage and negligible reactivity over time of the paste with B400 suggests that this binder was only partially dehydrated and not depolymerised. Thus, its elevated initial heat release may be ascribed to the rehydration of C-S-H, indicating that its hydration mechanism was an immediate rehydration of the dehydrated phases, instead of a dissolution-precipitation mechanism similar to that of CEM I. On the other hand, the reduced hydration heat release of the paste with B900 should be associated with the lower reactivity of the $C_2S$ polymorphs formed at this temperature, as demonstrated by the XRD and $^{29}$Si-NMR analyses (Figs. 2 and 3).

In general, the RB pastes exhibited more extended induction, acceleration and deceleration periods with diminished hydration heat release compared to those of the CEM I paste, and in spite of having presented higher initial hydration heat, they should develop less long-term hydration reactions than the CEM I paste, as suggested in the TG analysis (Table 2).

### 3.6. Compressive strength

Figure 5 presents the compressive strength at 3 and at 28 days of PNT and PB400-PB900. Similarly to CEM I pastes, the compressive strength of RB pastes increased from 3 to 28 days, independently of the treatment temperature. At 28 days, the compressive strength of the RB pastes varied between 4.1 MPa and 18.3 MPa, having increased with the treatment temperature up to 800ºC (Fig. 5), despite the increment of the w/b. Similar findings were presented by other authors (Shui et al., 2009; Vyšvaril et al., 2014).

The reduced compressive strength of PB400-PB500 should be owed to the fact that the RB particles were yet to be depolymerised and only dehydrated. Thus, given that the rehydration took place in a previously established structure, the formation of supplementary bonds between particles was not significant, with no relevant contribution to an overall gain of cohesion and the consequent increase of compressive strength.

Over 600ºC, the compressive strength of RB pastes increased significantly, as a result of the gradual depolymerisation of the RB with the thermal activation (Fig. 3), forming new anhydrous $C_2S$ polymorphs, which should exhibit quick rehydration ability. On the other hand, over 700 ºC, a general reduction of the compressive strength of RB pastes of identical consistency with the treatment temperature occurred, owed to the possible reduction of the surface area of RB particles and decreased reactivity of the polymorph $\beta$-$C_2S$, formed at this range of temperatures (Fig. 2). In fact, the compressive strength of PB900 at 3 days was around 10 times lower than those of PB600-PB800, even when the w/b was similar (PB800).

The compressive strength evolution from 3 to 28 days tended to be more significant in pastes with RB treated over 700 ºC (Fig. 5), which is consistent with the formation of $C_2S$ polymorphs of lower reactivity, as observed in the XRD analysis (Fig. 2). The compressive strength of PNT was not noteworthy (Fig. 5), demonstrating the importance of thermal activation to the rehydration capacity of cement. The little strength developed by PNT should be owed to the hydration of residual anhydrous CEM I particles present in NT.

Figure 6 displays the evolution of the compressive strength up to 90 days of PC0.72, PB600 and PB700 with comparable w/b. Up to 3 days, the compressive strength of these pastes was identical. However, over 3 days, their mechanical performance was lower than that of PC0.72. In fact, the compressive strength at 28 days was about 73% of that of PC0.72.

As mentioned by other authors, the quick early strength improvement of PB600 and PB700 may be ascribed to the elevated surface area of RB particles (Baldusco et al., 2019; Bogas et al., 2019; Shui et al., 2009). Furthermore, a portion of the mixing water should be firstly employed on the development of internal hydration products inside the RB particle porosity, lowering the available water amongst anhydrous particles. Consequently, the bulk RB paste should resemble a lower w/b paste, increasing particle proximity and accelerating their cohesion, thus enhancing early mechanical strength. In fact, at 1 day, the compressive strength of B600 was about 1.4 times higher than that of PC0.72 (Fig. 6). Nonetheless, non-porous CEM I pastes tend to produce a higher amount of external hydration products over time, reversing the tendency, which, in this case, took place at 3 days. Additionally, the porous RB pastes have been reported to be limited by a strength threshold (Fig. 6), hindering long term mechanical strength evolution (Zhang et al., 2018).

The compressive strength of PC0.31 (80.1 MPa at 28 days) was up to 6 times higher than those of B600-B900 of the same consistency, primarily due to the considerably lower w/b of PC0.31.

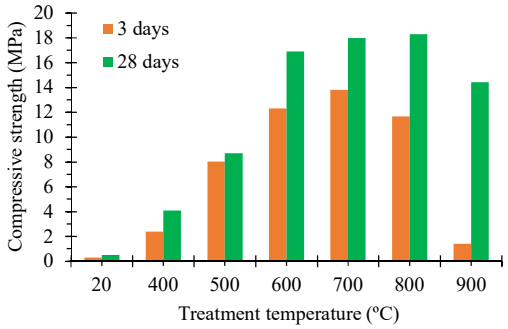


Figure 5. Compressive strength at 3 and 28 days of PNT and PB400-PB900

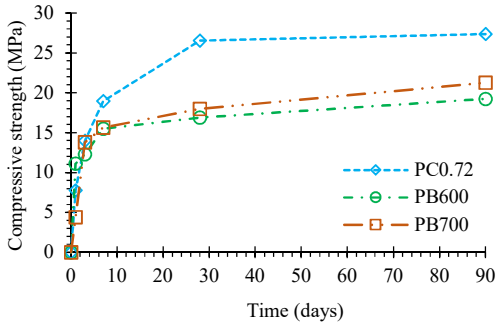


Figure 6. Compressive strength up to 90 days of PC0.72, PB600 and PB700

## 4. Conclusions

This paper characterised the rehydration behaviour and compressive strength of recycled cement binders subjected to treatment temperatures between 400 and 900ºC.

The XRD and $^{29}$Si-NMR analyses of RB demonstrated the effective depolymerisation of C-S-H and the formation of different $C_2S$ polymorphs, over 600 ºC. At 600-700 ºC, the polymorph $\alpha'_L$-$C_2S$ was identified as the main $C_2S$ polymorph present in this binder. Over 800 ºC, the polymorph $\beta$-$C_2S$ was also identified and, thus, the reactivity of these RB was slower. At 400-500 ºC, the C-S-H in the RB was dehydrated, though not fully depolymerised.

The elevated hydration heat release of the RB treated over 600 ºC confirmed the high reactivity of the compounds formed during thermal treatment. However, despite having displayed higher initial hydration heat, the RB presented lower long-term reactivity than CEM I.

The water demand of the RB pastes increased with the treatment temperature, having been up to 3 times higher than that of the CEM I paste. Furthermore, the setting times of RB were over 2 times higher than that of CEM I, having increased with the treatment temperature.

In sum, from the experimental characterisation of the thermoactivated recycled cement binders, the optimal thermal activation temperature was 700 ºC, at which the decarbonation stage of cement production is also mostly avoided. Finally, the compressive strength of the RB pastes was up to 42% higher at 1 day and over 31% lower at 28 days than that of the CEM I paste of similar w/b.

## Acknowledgements

The authors wish to thank the Portuguese Foundation for Science and Technology (FCT), for funding this research under project PTDC/ECI-COM-28308/2017. The authors would like to acknowledge the

support of CERIS/IST and CeFEMA/IST as well as thank SECIL, for suppling the CEM I 42.5R for the experimental campaign, and Professor Manuel Francisco Costa Pereira (IST), Professor Ana Paula Soares Dias (IST) and Eng. Miguel Carvalho, for their collaboration on the experimental work. The second author also wishes to thank the financial support of FCT through scholarship SFRH/BD/146033/2019.

## References

Alonso, C., Fernandez, L., 2004. Dehydration and rehydration processes of cement paste exposed to high temperature environments. J. Mater. Sci. 39, 3015–3024.

Angulo, S., Guilge, M., Quarcioni, V., Baldusco, R., Cincotto, M., 2013. Rehydration of cement fines: A TG/calorimetry study. Institute for Technological Research, São Paulo.

Baldusco, R., Nobre, T., Angulo, S., Quarcioni, V., Cincotto, M., 2019. Dehydration and rehydration of blast furnace slag cement. J. Mater. Civ. Eng. 31, 04019132.

Bogas, J.A., Carriço, A., Pereira, M.F.C., 2019. Mechanical characterization of thermal activated low-carbon recycled cement mortars. J. Clean. Prod. 218, 377–389. https://doi.org/10.1016/j.jclepro.2019.01.325

Carriço, A., Real, S., Bogas, J., Pereira, M., 2020. Mortars with thermoactivated recycled cement: fresh and mechanical characterisation. Constr. Build. Mater. 256, 119502.

EN 1015-11, 2000. Methods of test for mortar for masonry. Part 11: Determination of flexural and compressive strength of hardened mortar. European Committee for standardization (CEN).

EN 196-11, 2018. Methods of testing cement. Part 11: Heat of hydration. Isothermal Conduction Calorimetry method. European Committee for standardization (CEN).

EN 196-3, 2016. Methods of testing cement. Part 3: Determination of setting times and soundness. European Committee for standardization (CEN).

Grimmer, A., Von Lampe, F., Mägi, M., Lippmaa, E., 1985. High-resolution solid-state 29Si NMR polymorphs of Ca2SiO4. Cem. Concr. Res. 15, 467–473.

Hong, S.-H., Young, J., 1999. Hydration kinetics and phase stability of dicalcium silicate synthesized by the pechini process. J. Am. Ceram. Soc. 82, 1681–1686.

Lü, L., He, Y., Hu, S., 2008. Structural characteristics of dehydrated phase of hardened cement paste and its rehydrating ability. J. Chinese Ceram. Soc. 36, 1343–1347.

Serpell, R., Lopez, M., 2015. Properties of mortars produced with reactivated cementitious materials. Cem. Concr. Compos. 64, 16–26. https://doi.org/10.1016/j.cemconcomp.2015.08.003

Serpell, R., Zunino, F., 2017. Recycling of hydrated cement pastes by synthesis of α ′ H -C 2 S. Cem. Concr. Res. 100, 398–412. https://doi.org/10.1016/j.cemconres.2017.08.001

Shui, Z., Lu, J., Tian, S., Shen, P., Ding, S., 2014. Preparation of new cementitious system using fly ash and dehydratd autoclaved aerated concrete. J. Wuhan Univ. Technol. Sci Ed 29, 726–732.

Shui, Z., Xuan, D., Chen, W., Yu, R., Zhang, R., 2009. Cementitious characteristics of hydrated cement paste subjected to various dehydration temperatures. Constr. Build. Mater. 23, 531–537. https://doi.org/10.1016/j.conbuildmat.2007.10.016

Skibsted, J., 2016. High-resolution solid-state nuclear magnetic resonance spectroscopy of portland cement-based systems. In A Practical Guide to Microstructural Analysis of Cementitious Materials. Edited by Scrivener K, Snellings R, Lothenbach B. CRC Press. Taylor & Francis Group.

Vyšvaril, M., Bayer, P., Chromá, M., Rovnaníková, P., 2014. Physico-mechanical and microstructural properties of rehydrated blended cement pastes. Constr. Build. Mater. 54, 413–420. https://doi.org/10.1016/j.conbuildmat.2013.12.021

Wang, J., Mu, M., Liu, Y., 2018. Recycled cement. Constr. Build. Mater. 190, 1124–1132. https://doi.org/10.1016/j.conbuildmat.2018.09.181

Yu, R., Shui, Z., 2013. Influence of agglomeration of a recycled cement additive on the hydration and microstructure development of cement based materials. Constr. Build. Mater. 49, 841–851. https://doi.org/10.1016/j.conbuildmat.2013.09.004

Zhang, L., Ji, Y., Huang, G., Li, J., Hu, Y., 2018. Modification and enhancement of mechanical properties of dehydrated cement paste using ground granulated blast-furnace slag. Constr. Build. Mater. 164, 525–534. https://doi.org/10.1016/j.conbuildmat.2017.12.232